

BAR-ILAN UNIVERSITY

**From Interdependent Superconducting Networks to Single
Layer Two Interactions Systems**

Yuval Sallem

Submitted in partial fulfillment of the requirements for the Master's
Degree in the Department of Physics

Bar-Ilan University

Ramat-Gan, Israel

2025

This work was carried out under the supervision of Prof. Aviad Frydman
Department of Physics, Bar-Ilan University.

Contents

1	Abstract	1
2	Introduction	2
2.1	Phase Transitions	2
2.2	Interdependent Networks	3
2.3	Interdependent Superconducting Networks	5
2.3.1	The effect of dependency	5
2.3.2	Dynamics	7
3	Motivation and Objectives	10
4	Experimental Methods	11
4.1	Fabrication	11
4.1.1	The basic superconducting network	11
4.1.2	Substrate	11
4.1.3	Samples	12
4.2	Measurements	13
4.2.1	Transport Measurements	13
4.2.2	Dynamic Measurement	14
5	Results	15
5.1	A Single Superconducting Network Compared to Interdependent Superconducting Networks	15
5.1.1	Transport	15
5.1.2	Dynamics	16
5.2	Size Dependence	18
5.3	Superconducting Networks on Different Substrates	20
6	Discussion and Conclusions	24
7	Future Research	29
8	Appendix	31
	Reference	32

List of Figures

2.1	Different orders of phase transitions	3
2.2	Two-interaction system	4
2.3	Network functionality	4
2.4	Interdependent superconducting networks system	5
2.5	Experimental $R(T)$ measurements for different bias currents	6
2.6	System approaching criticality	7
2.7	Plateau dynamics	8
2.8	System collapse	9
4.1	Superconducting network	11
4.2	TISS and ISN	12
4.3	Illustration of sample configurations	13
4.4	Dynamic measurement	14
5.1	ISN versus TISS transport measurements	15
5.2	Dynamics	17
5.3	Dependency at different system sizes	18
5.4	System size scaling	19
5.5	Dependency via substrate	20
5.6	Dependency strength	21
5.7	Substrate dependence	22
5.8	Critical temperatures	23
6.1	Heat flow	27
8.1	Tuning the PT	31

1 Abstract

Phase transitions in complex systems often arise from the interplay of multiple interactions between elements. Interdependent network theory predicts that when two types of interactions, connectivity and dependency, coexist, systems can display mixed-order transitions, characterized by both abrupt discontinuities and critical scaling. While this phenomenon has been experimentally demonstrated in interdependent superconducting networks (ISN), its emergence in single network systems has remained unexplored.

In this work, we investigate single network systems, which consist of a single disordered indium-oxide network where electric current provides connectivity and Joule heating generates effective dependency among segments. Using transport and dynamic resistance measurements, we show that these Two-Interaction Superconducting Systems (TISS) reproduce the key features of ISN: abrupt and hysteretic transitions, long-lived plateaus in the dynamics near criticality, and universal critical exponents ($\beta = 1/2$, $\zeta = 1/2$, $\psi = 1/3$). Comparison of ISN and TISS demonstrates that the existence of dual interactions alone in a system is sufficient to induce mixed-order transitions, even without structurally distinct networks.

We further demonstrate that the substrate thermal conductivity provides a powerful control parameter for tuning dependency interactions. Glass substrates, with low thermal conductivity, enhance heat retention and induce abrupt transitions at relatively low driving currents, while silicon substrates, with higher thermal conductivity, require higher currents to exhibit similar behavior. These observations confirm the thermal origin of dependency interactions in these superconducting systems and establish substrate engineering as a means of controlling its robustness near criticality.

Altogether, this work positions TISS as a controllable platform for studying interdependency, highlights the universality of mixed-order transitions, and suggests broader applications in systems where dual interactions naturally emerge, from neural and traffic networks to device-oriented phase-switching technologies.

2 Introduction

2.1 Phase Transitions

Phase transitions (PTs) are among the most captivating and fundamental phenomena in statistical physics, manifesting across a wide range of physical systems and natural processes. Traditionally, classical PTs are thermally driven, with temperature acting as the key tuning parameter. For instance, below a critical temperature T_c , liquid water may crystallize into ice, a non-magnetic material can spontaneously develop magnetic order and become a ferromagnet, a normal metal can become superconducting, etc.

PTs are typically classified into two primary categories based on their thermodynamic and macroscopic behavior near the critical point [1, 2]. In a *first-order* PT, such as the melting of a solid or the boiling of a liquid, the transition is discontinuous, as the order parameter changes abruptly, and the system either absorbs or releases latent heat. These transitions are often accompanied by hysteresis, as the system is heating or cooling (see Fig. 2.1a).

In contrast, *second-order* (or continuous) PTs, such as the normal-superconductor transition or the paramagnetic-ferromagnetic transition, are characterized by a smooth and continuous change of the order parameter at the critical point (see Fig. 2.1b). As the system approaches criticality from either side (i.e, cooling or heating), it exhibits critical behavior accompanied by set of universal features such as scaling laws and critical exponents [3, 4].

In addition, less common transitions, known as mixed-order, also exist. transitions. These transitions combine features of both first, and second order PTs. They exhibit a discontinuous jump in the order parameter and hysteresis, characteristic of first-order transitions, but also display critical behavior, such as scaling laws, on approach to the transition point, akin to second-order transitions (see Fig. 2.1c).

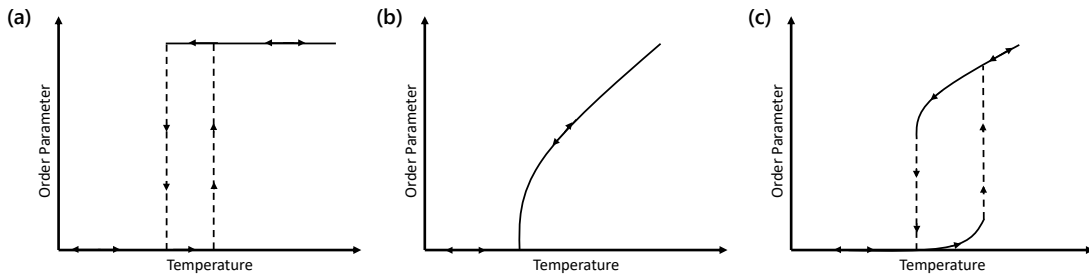


Figure 2.1: Different orders of phase transitions

2.2 Interdependent Networks

Understanding networks is important in our modern age. Networks are embedded in our civilization and appear everywhere in our lives. From power grids, communication, the Internet, and train rails to neuroscience, AI modules, stock markets, and more. Although these networks may seem isolated, in many cases they are connected to each other and can depend on one another (i.e., they are coupled). For example, a power station relies on the internet so it could communicate with other stations, while the internet itself relies on electricity. This coupling reduces the robustness of each network by making it more vulnerable to local failures [5].

This understanding was absent in conventional network research until 2010, when Havlin published his seminal article [6], which paved the way to the new field of *networks of networks* [7–9]. The main innovation introduced by Havlin was the concept of *dependency*, emerging from interactions between networks. His theory hinges on two types of interactions in a system of networks (see Fig. 2.2).

1. **Connectivity** – Interaction between nodes within the *same* network, enabling information to propagate throughout the network (e.g., electric current in a conductive lattice).
2. **Dependency** – Interaction between nodes in *different* networks (e.g., heat dissipation between conducting films). If a node in one network fails, the node depending on it in the other network also fails.

The model system for this theory is percolating networks. Here, the relevant order parameter is the giant component P_∞ , which represents the largest cluster of connected and functioning nodes. For a single-network system, characterized by one interaction (i.e., connectivity), the giant component follows:

$$P_\infty = p[1 - \exp(-\bar{k}P_\infty)] \quad (1)$$

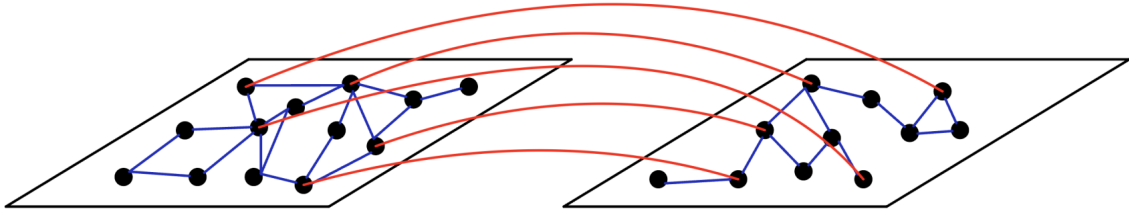


Figure 2.2: Two-interaction system – Blue lines represent connectivity interactions, while red lines represent dependency interactions.

where p is the fraction of functioning nodes, and \bar{k} is the average degree of the network, indicating the average number of connections each node has [8]. The solutions of Eq. 1 are shown in Fig. 2.3 (black curve), for $\bar{k} = 5$. This result yields a continuous second-order PT with

$$p_c = 1/\bar{k} \quad (2)$$

where p_c is the critical value of p , below which the network gets fragmented and collapses.

For a multi-network system, characterized by two interactions (i.e., connectivity and dependency), Eq. 1 is replaced by

$$P_\infty = p[1 - \exp(-\bar{k}P_\infty)]^n \quad (3)$$

where n is the number of interdependent networks comprising the system [8]. The solutions of Eq. 3 are shown in Fig. 2.3 (red curves). For any $n > 1$, the order parameter P_∞ becomes discontinuous, corresponding to a first-order PT, while critical behavior is exhibited as the system approaches criticality, corresponding to a second-order PT. Hence, this unique PT is of mixed-order.

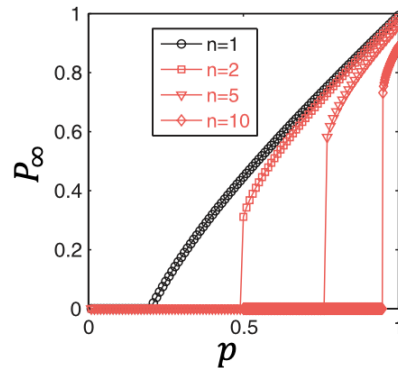


Figure 2.3: Network functionality – The giant component P_∞ as a function of the fraction of functioning nodes p , for different numbers of interdependent networks n [5].

2.3 Interdependent Superconducting Networks

Since 2010, Havlin and others have continued to develop interdependent network theory and applied it to a variety of interdependent systems [10–21]. However, none of these were able to test the theory on a controllable, real physical system.

Our group developed the first real solid-state physical system of interdependent networks, in the form of two disordered superconducting networks, separated by an electrical insulator that is a good heat conductor, as seen in Fig. 2.4 [22]. The disorder in the superconducting networks causes a spread of critical temperatures T_c and critical currents I_c . In this system, electric current driven through each network creates connectivity within the networks, while Joule heating of segments between the networks creates dependency.

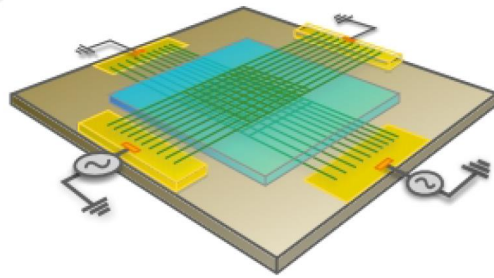


Figure 2.4: Interdependent superconducting networks system – Two networks (in green), separated by a thermally conducting insulating medium (in blue). Edges of each network are connected to gold contacts to enable transport measurements [22].

2.3.1 The effect of dependency

Experimental results [22] for resistance versus temperature measurements of interdependent superconducting networks (ISN) are presented in Fig. 2.5. When the two networks are measured *separately* (see Fig. 2.5a), a continuous second-order PT is observed, from the normal phase (N) to the superconducting phase (S) and back, for both low ($I_b < 10 \mu\text{A}$) and high ($I_b > 10 \mu\text{A}$) bias currents. This behavior changes when the networks are measured *simultaneously* (see Fig. 2.5b). In this case, for low currents, the behavior is similar to the separate case, but for higher currents, generating sufficient heat, a mutual, abrupt, discontinuous, and hysteretic PT is observed. This transition is accompanied by critical behavior as the system approaches the critical point.

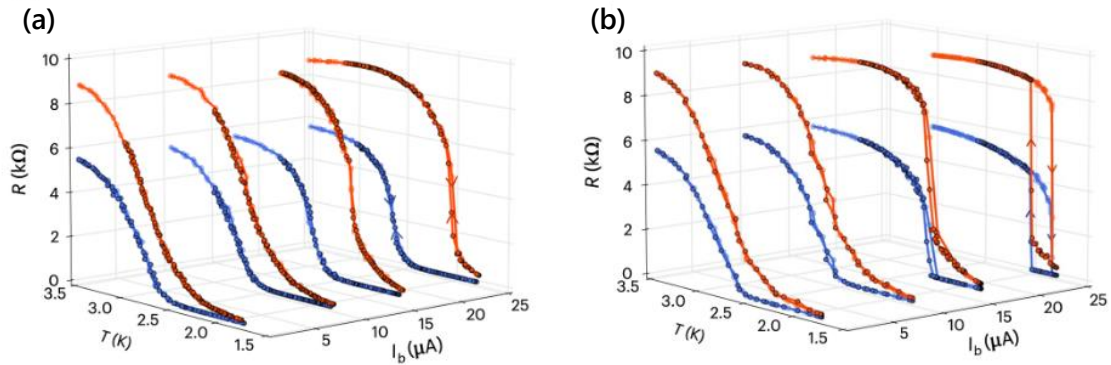


Figure 2.5: Experimental $R(T)$ measurements for different bias currents – Top network in red, bottom network in blue. Arrows indicate heating or cooling cycles. **(a)** Measurements performed on each network separately. No dependency is exhibited, and a continuous, second-order PT is observed. **(b)** Measurements performed on both networks simultaneously. For low currents, not enough heat is generated to induce dependency, and the behavior is similar to that of two single networks. For currents above $15 \mu A$, sufficient heat is produced to couple the networks, resulting in an abrupt, discontinuous, and hysteretic PT [22].

Near the N to S transition, the $R(T)$ curve was found to follow:

$$R(T) - R(T_c) \propto |T - T_c|^\beta \quad (4)$$

with $\beta = 1/2$ [23]. Additional study [23] was performed on these systems by measuring resistance versus current, as shown in Fig. 2.6. Here, the temperature is kept constant at $T < T_c$, while the bias current is swept through I_c . Similarly to the $R(T)$ curves, an abrupt, hysteretic PT is observed, accompanied with the same critical behavior and scaling laws. Near the N to S transition, the $R(I_b)$ curve was found to follow:

$$R(I_b) - R(I_c) \propto |I_b - I_c|^\beta \quad (5)$$

with both experimental measurements (Fig. 2.6a) and numerical calculations (Fig. 2.6b) yielding $\beta = 1/2$ [23], as shown in the insets of Fig. 2.6.

This result aligns precisely with theoretical predictions and numerical simulations of percolation on abstract interdependent networks [24] and simulations of interdependent ferromagnetic networks [25]. The consistent appearance of this critical exponent in various systems may indicate a universal mechanism associated with the presence of two interactions in a system.

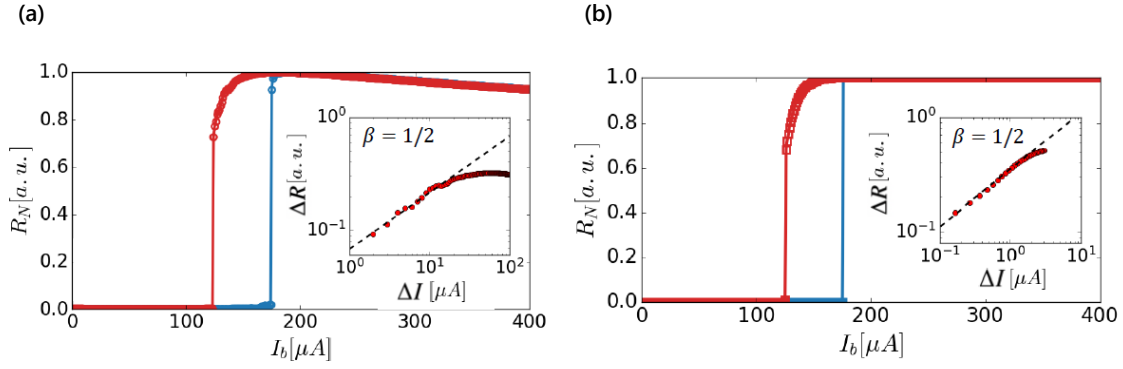


Figure 2.6: System approaching criticality – Experimental measurements (a) and numerical simulations (b) of $R(I_b)$ curves approaching the critical point. Blue and red lines represent increasing and decreasing currents, respectively. Insets show the extraction of the critical exponent $\beta = 1/2$ from the N to S PT (red curves) [23].

2.3.2 Dynamics

Identifying the underlying physical mechanisms of a PT is essential to understand its nature. A recent research [23] unravels the microscopic origin of this abrupt transition. The dynamics of the system (i.e. resistance versus time) was measured at criticality, during the N to S PT. The results shown in Fig. 2.7 are based on the following protocol: (i) The system is controlled and fixed at a temperature $T < T_c$ and the bias current is set at $I_b > I_c$ so the system is tuned to be in the N-state. (ii) At time $t = 0$ the current is abruptly switched to a value $I_b < I_c$ and $R(t)$ is measured. Remarkably, when the bias current is switched very close to the critical current $I_b \rightarrow I_c$, the resistance curves display a semi-saturated resistance for a long time (long-term plateau) before it drops abruptly to zero resistance as the system transits to the S-state (Fig. 2.7a,c show experimental and numerical results respectively). The time, τ , of this *plateau* can last for *thousands* of seconds, many orders of magnitudes longer than the timescales of electronic interactions ($\tau_e \sim 10^{-12} - 10^{-10} s$) within each network or phonon between them ($\tau_p \sim 10^{-8} - 10^{-6} s$), indicating that the interplay between the layers plays a significant role in the process. The inset of Fig. 2.7a is a zoom in on the plateau regime, showing that the resistance does not monotonically decrease with time but fluctuates. The process above is repeated by deep quenching to slightly lower values of I_b . It is found that, as I_b decreases, τ decreases as well (Fig. 2.7a). The measured plateau duration time τ is found to follow a scaling behavior with the distance of the bias current from the critical current as

$$\tau \propto |I_b - I_c|^{-\zeta} \quad (6)$$

with an exponent of $\zeta = 1/2$ as seen in Fig. 2.7b,e for experimental and numerical results respectively. This value is consistent with the theoretical prediction for percolation on abstract interdependent networks [26].

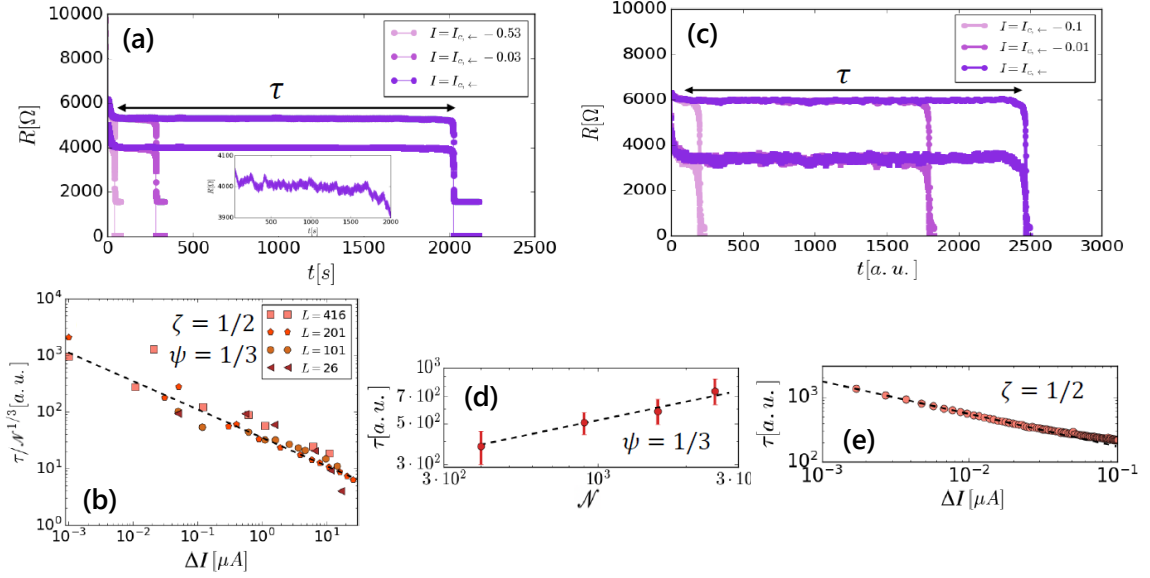


Figure 2.7: Plateau dynamics – Experimental measurements (a) and numerical simulations (b) of resistance versus time for different currents during the collapse from N to S. As the currents approach the critical value, the duration of the plateau τ increases. The inset of (a) zooms in on the plateau regime, showing that the resistance slightly decreases with time. (c) Experimental measurements for various system sizes $N = L \times L$ exhibit exponents $\zeta = 1/2$ and $\psi = 1/3$, in excellent agreement with numerical simulations (d–e) [23].

The extremely long plateau indicates a mechanism of spontaneous long-term microscopic changes. It suggests that due to the long-range dependency (heat) in such ISNs, each segment in one network may influence every segment in the second network. Thus, the interactions become nearly spatially random where, near criticality, phase changes (N-S) of elements are generated anywhere in the system depending on T_c and I_c of the individual segments. In this near criticality regime, the PT is governed by a spontaneous microscopic *random-cascading*, i.e. a chain of events where one element, that has changed its phase, influences on average one element at a different location with closest T_c and I_c in the other network due to thermal dissipation. This process continues until enough elements undergo a phase-change thus causing a macroscopic PT. While the results focuses on the transition from N to S, an analogous process is expected to occur for a transition from S to N, as illustrated in Fig. 2.8. Since the changes during the plateau are microscopic, in order to influence the whole system, it is reasonable to expect τ to depend on the system

size (i.e. the number of segments). For this, the time duration of the plateau, τ , for different system sizes is measured. Fig. 2.7b,d shows experimental measurements and numerical simulations of the dependence of τ on the system size which follows

$$\tau \propto N^\psi \quad (7)$$

where N is the number of segments in a system and $\psi = 1/3$. This scaling law and exponent were also observed in percolation on abstract interdependent networks [26]. This result supports the paradigm that the plateau, during the abrupt transition, represents a *microscopic* process that occurs spontaneously for a *macroscopic* time. The collapse of all experimental curves in the plot of Fig. 2.7b supports the interpretation of the slowing down resulting from critical branching.

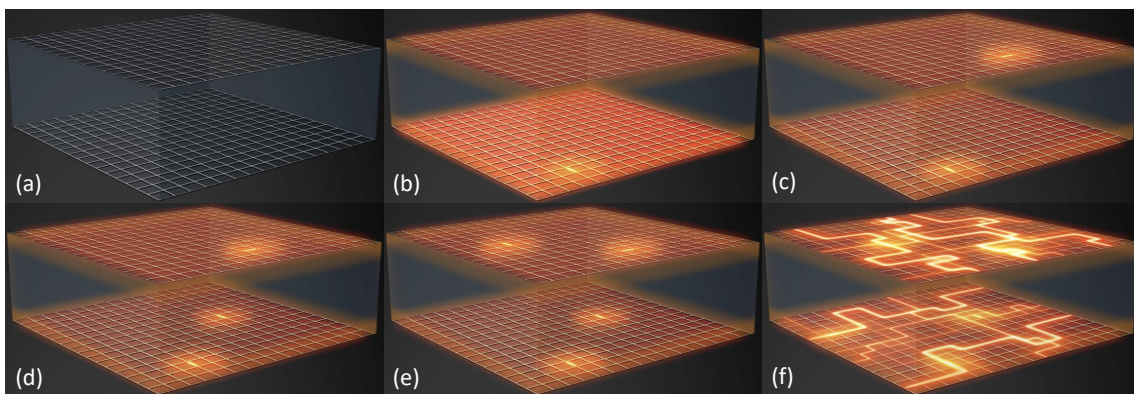


Figure 2.8: System collapse - At $t = t_0$ all segments are at the S-state **(a)**. When $t = t_1$, where $t_1 > t_0$, the weakest segment (with the lowest I_c and T_c) becomes normal **(b)** and start emitting heat throughout the system. At $t = t_2$, where $t_2 > t_1$, the next weakest segment in the *other* network becomes normal **(c)**. This process creates an avalanche of segments becoming normal one by one **(d-e)** until a critical amount is reached and both networks collapse **(f)** into the N-state abruptly.

3 Motivation and Objectives

Until now, research on ISN has focused on systems consisting of two networks stacked one on top of the other. In these systems, connectivity interactions are generated by the electric current driven through each network, and dependency interactions are generated by Joule heating of segments between the networks. In general, there is no reason to assume that heat is restricted to propagate solely *between* the two networks and cannot also affect each individual network. This led us to propose that the same concepts of ISN could be relevant for single-layer superconducting network systems that are characterized by two types of interactions. We dub these systems *Two-Interaction Superconducting System* (TISS).

Our first objective was to compare the behaviors of ISN and TISS, both qualitatively and quantitatively. Unlike interdependent networks, the manifestation of two interactions in single systems is much simpler and broader. Such systems are more abundant in nature, and their applications can be more widely implemented. For example, they may be relevant to information overload, where connectivity is achieved by information flow and dependencies arise from the overload of certain hubs due to limited tolerance; traffic networks, where connectivity is created by roads and dependency by traffic jams; neural networks, where connectivity involves electric signals in the brain and dependency involves excitation caused by distant neurons; and even regular solids, where connectivity is via interatomic interactions and dependency arises from long-range phonons. Thus, introducing and controlling a second type of interaction within the same system has profound implications.

This leads to our second objective, which was to control the dependency interaction in our TISS. Unlike ISN systems, where dependency arises between separate networks, in TISSs the dependency interaction is generated by segments in *one* network heating segments in the *same* network. Hence, the substrate directly influences the strength and range of the dependency interaction. Achieving such control and showing how it hinges on the substrate is significance. First, it reinforces the assumption regarding the thermal origin of the dependency in our systems. In addition, it enables further research that focuses on the range of the dependency, which theory predicts has a great effect on the nature of the PT. Lastly, it paves the way for harnessing these systems for practical usage, such as developing sensitive sensors that relies on the abrupt transition and thus the strength of the dependency.

4 Experimental Methods

4.1 Fabrication

4.1.1 The basic superconducting network

Our network is shaped as a two-dimensional square lattice, as seen in Fig. 4.1b. The size of the lattice (i.e., the number of segments) is $N = L \times L$, where L is the number of horizontal or vertical stripes, each one having dimensions of $2 \mu\text{m}$ wide, $10 \mu\text{m}$ long (see Fig. 4.1c) and 50 nm thick.

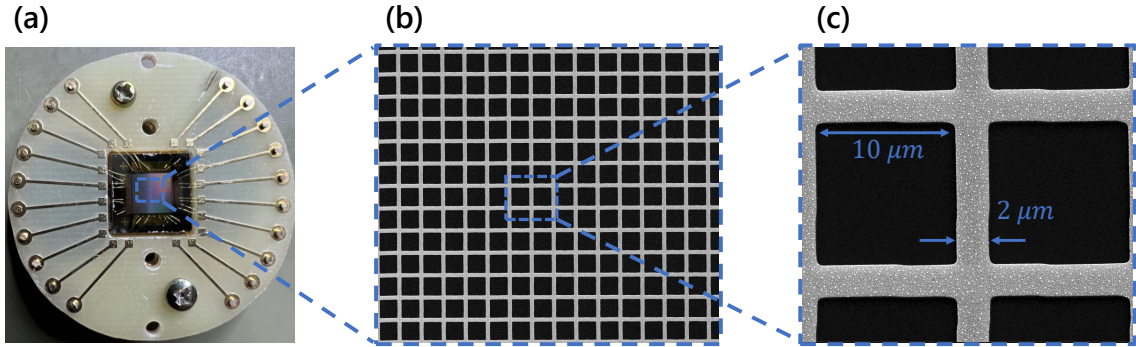


Figure 4.1: Superconducting network - (a) Sample attached to the holder and ready for measurement. (b–c) SEM images of the network taken at different magnifications.

The fabrication process begins with designing the desired network using a CAD program. We then use photolithography methods to create a mask in the shape of our design on a substrate. Following this, we e-beam evaporate, under a residual O_2 pressure of $6\text{--}8 \mu\text{Torr}$, a 50 nm -thick film of amorphous indium oxide (InO) onto the substrate. Under these conditions, the InO forms as a disordered superconductor, with a wide distribution of local T_c s and I_c s, and a bulk critical temperature of $T_c \approx 3 \text{ K}$.

4.1.2 Substrate

We used two types of substrates: undoped silicon and borosilicate glass. While both are excellent electrical insulators at cryogenic temperatures, they differ significantly in thermal conductivity. Silicon has a thermal conductivity of approximately $\kappa \approx 500 \frac{\text{W}}{\text{m}\cdot\text{K}}$ at $T = 2 \text{ K}$ [27], whereas glass has $\kappa \approx 0.01 \frac{\text{W}}{\text{m}\cdot\text{K}}$ at the same temperature [28]. This means that although silicon allows heat to spread more efficiently across the sample than glass, it also permits heat to escape to the heat bath (i.e., the cryostat) much more readily than the glass substrate.

4.1.3 Samples

As part of this research, we fabricated two types of systems. The first is a TISS (see Fig. 4.2a), comprising a single network of size $N = L \times L$, fabricated on one of the two substrates (i.e., silicon or glass). Au contacts made of 4 nm Cr and 40 nm Au were fabricated, using lithography, at the edges of the network to enable electrical transport measurements.

The second type is an ISN system. The fabrication process starts with a TISS sample. We then cover it with a 100 nm-thick film of aluminum oxide (AlO), which is thermally conductive and electrically insulating. Following this, we fabricate an identical network on top of the AlO. This configuration yields two electrically isolated networks that can exchange heat. Lastly we add Au contacts in the same way as for the bottom network (see Fig. 4.2c).

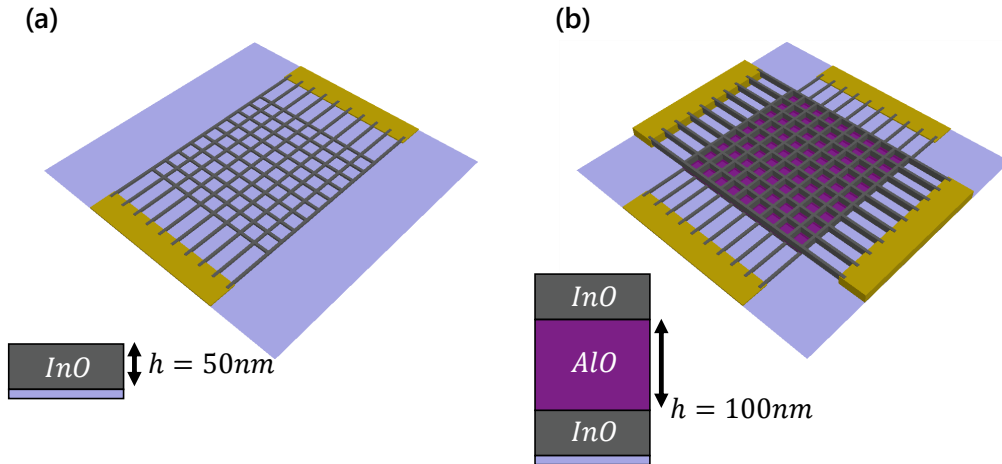


Figure 4.2: TISS and ISN - (a) **TISS**: A single InO network is fabricated on a thermally conducting and electrically insulating substrate. Au pads are placed on the sides of the network. (b) **ISN**: A layer of AlO, which is thermally conducting and electrically insulating, is deposited on top of a TISS sample. Then, an identical InO network is fabricated on top of the AlO. Au pads are placed on the sides of the top network.

Throughout this work, we fabricated three configuration of samples, as listed below.

- **S1** - TISS and ISN at size $N = 400 \times 400$ on two *separate* silicon substrates, as seen in Fig. 4.3a.
- **S2** - TISSs at sizes $N = 200 \times 200$, $N = 100 \times 100$, $N = 25 \times 25$ on the *same* silicon substrate, as seen in Fig. 4.3b.

- **S3** - Two separate samples of TISSs at sizes $N = 200 \times 200$ and $N = 25 \times 25$ on a silicon substrate, and a glass substrate, as seen in Fig. 4.3c.

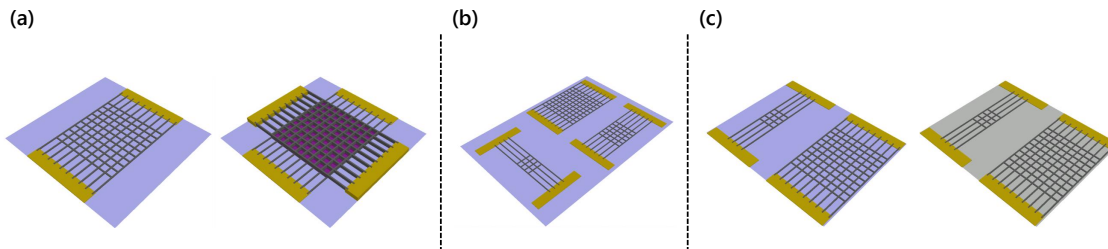


Figure 4.3: Illustration of sample configurations. (a) TISS and ISN system fabricated on two silicon substrates. (b) Three separate TISSs samples at different sizes patterned on a single silicon substrate. (c) Two TISSs at different sizes fabricated side-by-side on a shared substrate. Silicone is on the left, and glass is on the right.

4.2 Measurements

Since the bulk critical temperature of the sample is $T_c \approx 3$ K, we needed to achieve low temperatures. We used a RC102 cryostat that operates with a continuous flow of liquid helium. Helium liquefies at 4.2 K, so just submerging the sample inside a bath of it was not enough. By lowering the pressure inside the 1 K pot and having a continuous flow of liquid helium inside, a base temperature of $T_{\text{base}} < 1.8$ K was achieved. For good thermal insulation, the IVC was kept under high vacuum.

In all experiments, electric current was applied to each network using a Keithley 2410 sourcemeter, while voltage was measured using a Keithley 2000 multimeter. Sample temperature was controlled and measured using a LakeShore 330 controller, with a 25Ω heater and a DT-670 thermometer placed inside the cryostat, next to the sample.

4.2.1 Transport Measurements

Resistance as a function of temperature ($R(T)$) curves were obtained by driving a constant current through a network and measuring the voltage across it as the temperature varies within the range of $1.8 \text{ K} \leftrightarrow 6 \text{ K}$. This process is repeated for increasing values of current until an abrupt, hysteretic transition is observed. To extract the critical exponent β , we use a cooling $R(T)$ curve that exhibited such a transition. We subtract R_c and T_c from the resistance and temperature values, respectively. The values of R_c and T_c are selected to achieve the best linear behavior

on a log-log plot of $R - R_c$ as a function of $T - T_c$. The slope of this plot corresponds to the desired critical exponent β .

I - V characteristics were obtained by setting a network temperature to a fixed value below the critical temperature and measuring the voltage across it while sweeping the driven current through I_c . The extraction of the critical exponent β follows the same method as for the $R(T)$ curves, replacing the temperature with current.

4.2.2 Dynamic Measurement

For studying the dynamics of the N to S transition, we performed time-dependent resistance measurements. The measurement begins as we identify the critical current I_c of an N to S transition, from an $R(I)$ curve, as seen in Fig. 4.4a. We then measured the resistance as a function of time during the procedure shown in Fig. 4.4b: At $t = t_0$ we set the current of the system to a value deep inside the N-state. Then, at $t = t_1$, after the system stabilizes, we abruptly switch the current to a value, $I = I_c - \Delta I$, and measure the time τ it takes the system to collapse into the S-state. This process is repeated for decreasing ΔI until we exceed the critical current I_c and the system does not collapse anymore. To extract the critical exponent ζ , we plot τ as function of $I - I_c$, selecting I_c such that a log-log plot exhibits the best linear behavior. The slope of this plot is the desired ζ exponent.

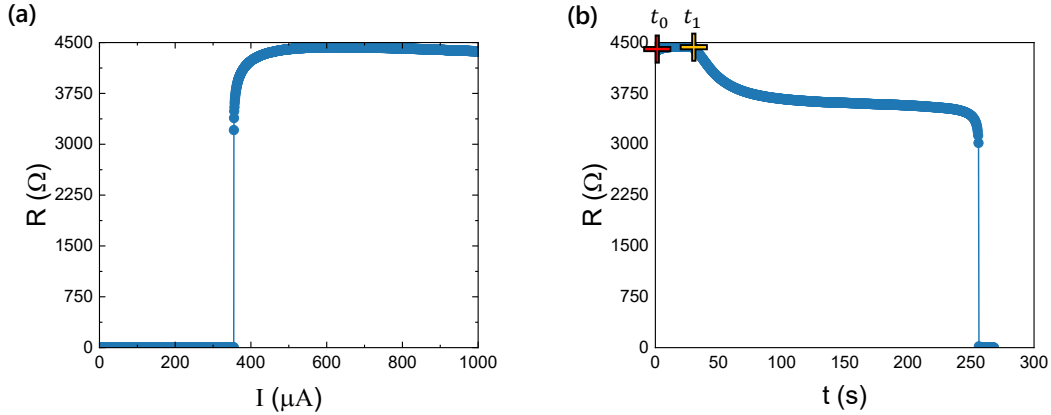


Figure 4.4: Dynamic measurement - (a) Resistance as a function of current ($R(I)$) during a sweep from the N-phase to the S-phase. (b) Resistance as a function of time ($R(t)$) during the time measurement.

5 Results

5.1 A Single Superconducting Network Compared to Interdependent Superconducting Networks

5.1.1 Transport

It was previously shown [22] that driving sufficient current through ISN results in an *abrupt* N–S PT, while driving the same current to only one of the networks results in a *continuous* transition. Here, we show that driving a high enough current through a *single* superconducting network (i.e., a TISS) results in an abrupt and hysteretic transition similar to those observed in ISN. This is demonstrated in Fig. 5.1, which compares the RT curves of an ISN system (Fig. 5.1a) and a TISS (Fig. 5.1b).

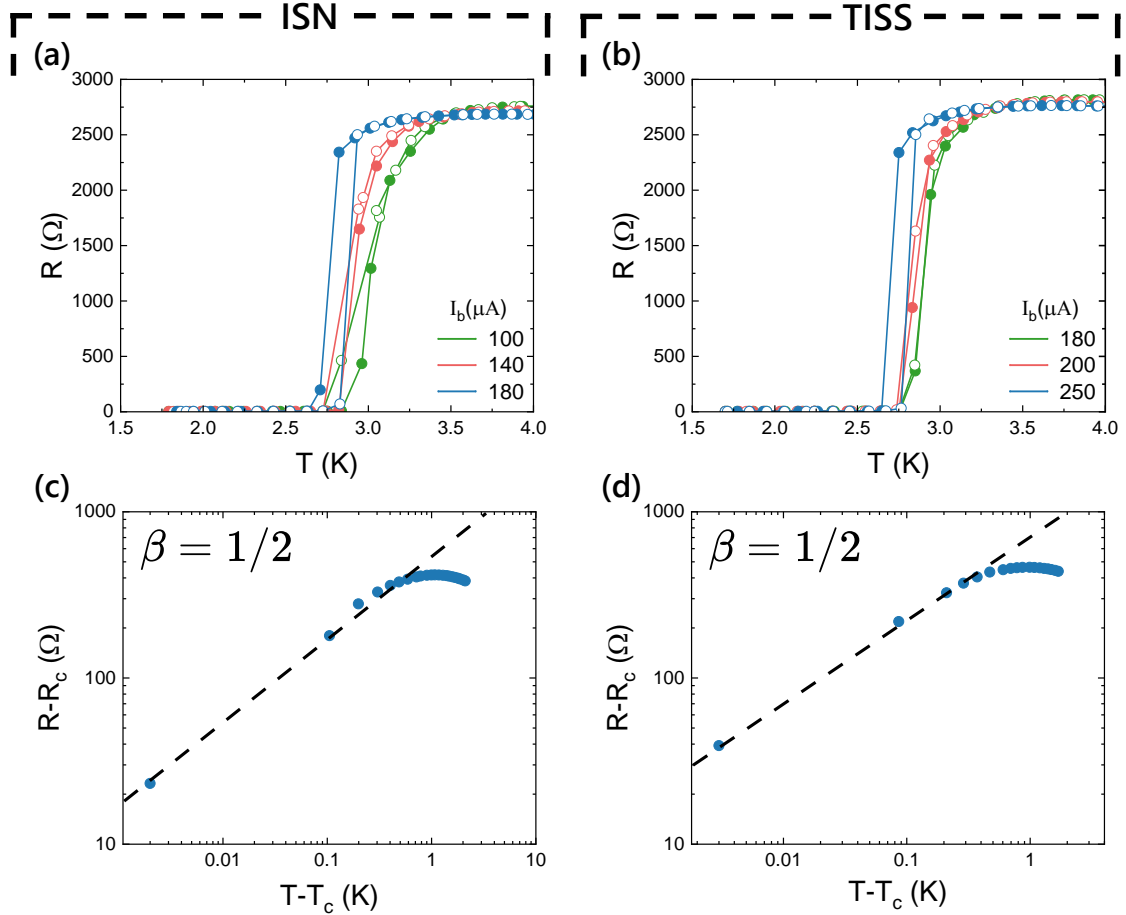


Figure 5.1: ISN versus TISS Transport measurements - Experimental resistance versus temperature measurements at different bias currents for ISN ($L = 400$) (a) and TISS ($L = 400$) (b). Full symbols are for cooling cycles, and empty symbols are for heating cycles. (c),(d) shows the extraction of the critical exponent $\beta = 1/2$ from the cooling curves of ISN and TISS for currents $I = 180 \mu\text{A}$ and $I = 250 \mu\text{A}$ respectively.

In both cases, for low currents (i.e., a single interaction system), the N–S and S–N transitions are continuous and occur without hysteresis. For high enough currents, where the second, thermal dependency interaction is generated, the transitions become abrupt and hysteretic. Notably, the TISS requires higher currents than ISN in order for dependency to be generated.

Furthermore, the results show that both TISS and ISN exhibit behaviors typical of mixed-order transitions, namely abrupt transitions accompanied by critical scaling. In particular, the critical exponent that describes the scaling of the resistance as the temperature approaches the critical point T_c (see Eq. 4) is found to be $\beta = 1/2$ for both samples, as shown in Fig. 5.1(c,d).

5.1.2 Dynamics

As stated in Section 2.3.2, the origin of the abrupt transition was found [23] to be microscopic in nature. This was demonstrated by measuring the dynamics of ISN during the PT. Fig. 5.2 shows resistance versus time measurements for ISN and TISS, following the same protocol as described in Section 4.2.2. It is seen that for both ISN (Fig. 5.2a) and TISS (Fig. 5.2b), when the driven current I is far from the critical value I_c , the collapse of the system, from the N-state to the S-state, lasts a few seconds. As the current increases ($I \rightarrow I_c$), and the systems get closer to criticality, the length of the collapse τ increases, and a long-lived plateau of the resistance with time is clearly observed. The length of the plateau could reach thousands of seconds, as seen in Fig. 5.2c,d. We note that during the plateau, the resistance does not decrease monotonically, but fluctuates, as seen in the corresponding insets.

Moreover, the critical exponent that governs the length of the plateau τ , as a function of the distance of the current I from the critical value I_c , as Eq. 6 describes, is found to be $\zeta = 1/2$ for both ISN (Fig.5.2e) and TISS (Fig.5.2f).

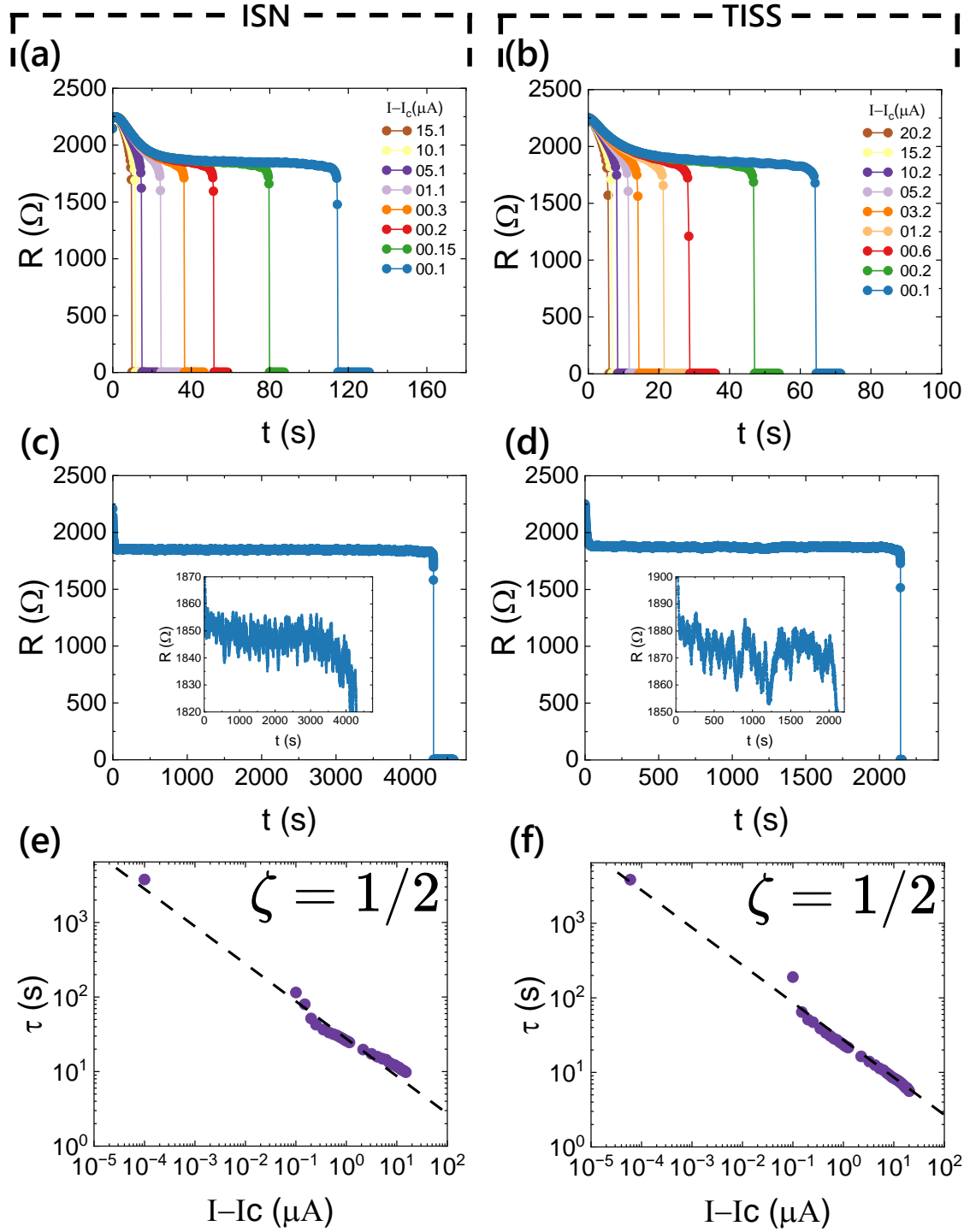


Figure 5.2: Dynamics - Resistance versus time measurements for driven currents gradually approaching the critical value for ISN ($L = 400$) (a) and TISS ($L = 400$) (b). (c),(d) resistance versus time for I very close to I_c demonstrating a plateau that lasts thousands of seconds. Insets shows fluctuations of the resistance with time. (e),(f) corresponding extracted values of ζ .

5.2 Size Dependence

In order to study if, and what effects a system size has on the properties of its PT, we first measured two TISSs of sizes $L = 25$ and $L = 400$. Results for resistance versus temperature measurements are presented in Fig. 5.3. It is seen that for both

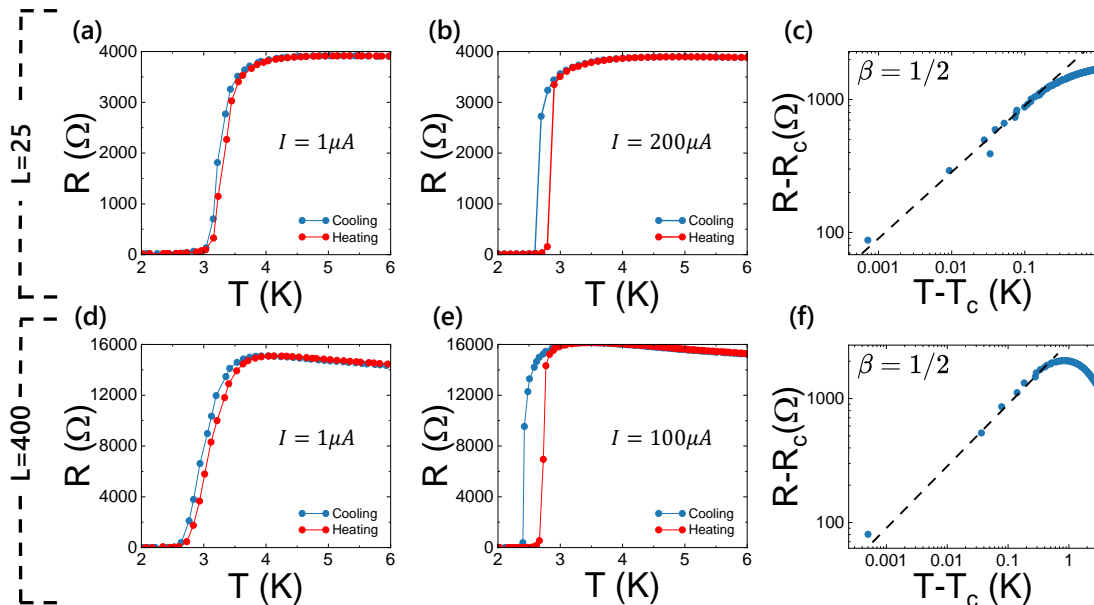


Figure 5.3: Dependency at different system sizes - Resistance versus temperature measurements for TISSs at sizes $L = 25$ and $L = 400$ at low currents ($I_{25} = I_{400} = 1 \mu A$) (a),(d) and high currents ($I_{25} = 200 \mu A$, $I_{400} = 100 \mu A$) (b),(e). (c),(f) shows the extraction of the critical exponent $\beta = 1/2$ from the corresponding cooling curves of (b),(e).

small (Fig. 5.3a) and large (Fig. 5.3d) systems, while the driven current is low and only negligible heat is generated, the transition is continuous. On the other hand, when the driven current is high enough and sufficient heat is generated, both small (Fig. 5.3b) and large (Fig. 5.3e) systems exhibit an abrupt transition accompanied by the same scaling laws and critical exponent as described by Eq. 4, with $\beta = 1/2$ (Fig. 5.3c,f), indicating an identical mixed-order transition, at different values of current.

In addition to RT measurements, we conducted dynamic measurements for TISSs with sizes $L = 25$, $L = 100$, and $L = 200$. The dependence of τ on $I - I_c$ and the network size is shown in Fig. 5.4.

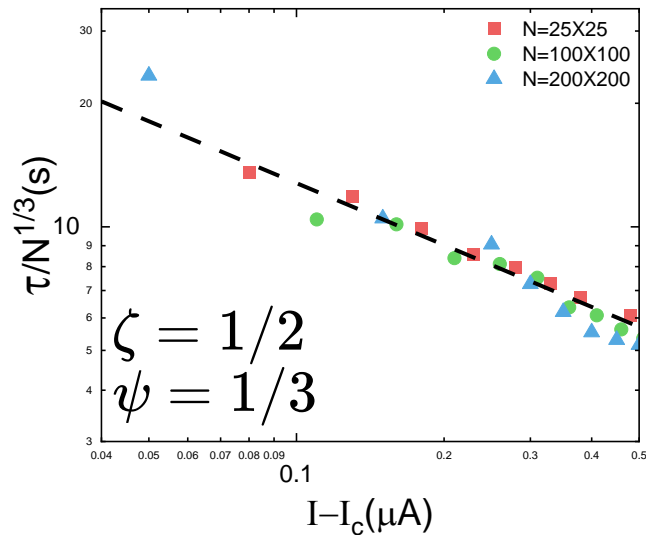


Figure 5.4: System size scaling - Scaled plateau duration versus the distance of a system from criticality, for TISSs of sizes $L = 25$, $L = 100$, and $L = 200$. Each of the three systems exhibits a scaling relation corresponding to Eq. 6 with $\zeta = 1/2$. The plateaus length scales with the size of the system, in agreement to Eq. 7, with $\psi = 1/3$.

It is seen that the plateau length τ scales with the distance of the current from the critical value I_c , according to Eq. 6, with $\zeta = 1/2$ for all systems. In addition, τ scales with the system size, in accordance with Eq. 7, with $\psi = 1/3$.

5.3 Superconducting Networks on Different Substrates

We have shown that a TISS behaves the same as ISN, as it exhibits the same PTs, dynamics, and critical scaling. In ISN, dependency is generated by the medium between the networks. We hypothesize that in a TISS, the substrate of the network (as well as the network itself) acts as this medium. In order to test the ability of the substrate to serve this cause, we show that two superconducting networks, fabricated side by side (see Fig. 4.3b,c and S2/S3 configurations), can become mutually coupled as a result of the heat dissipation of their shared substrate. Results for resistance versus current measurements, for networks of size $L = 25$ and $L = 100$, are presented in Fig. 5.5. When the two networks are measured *separately*, they both

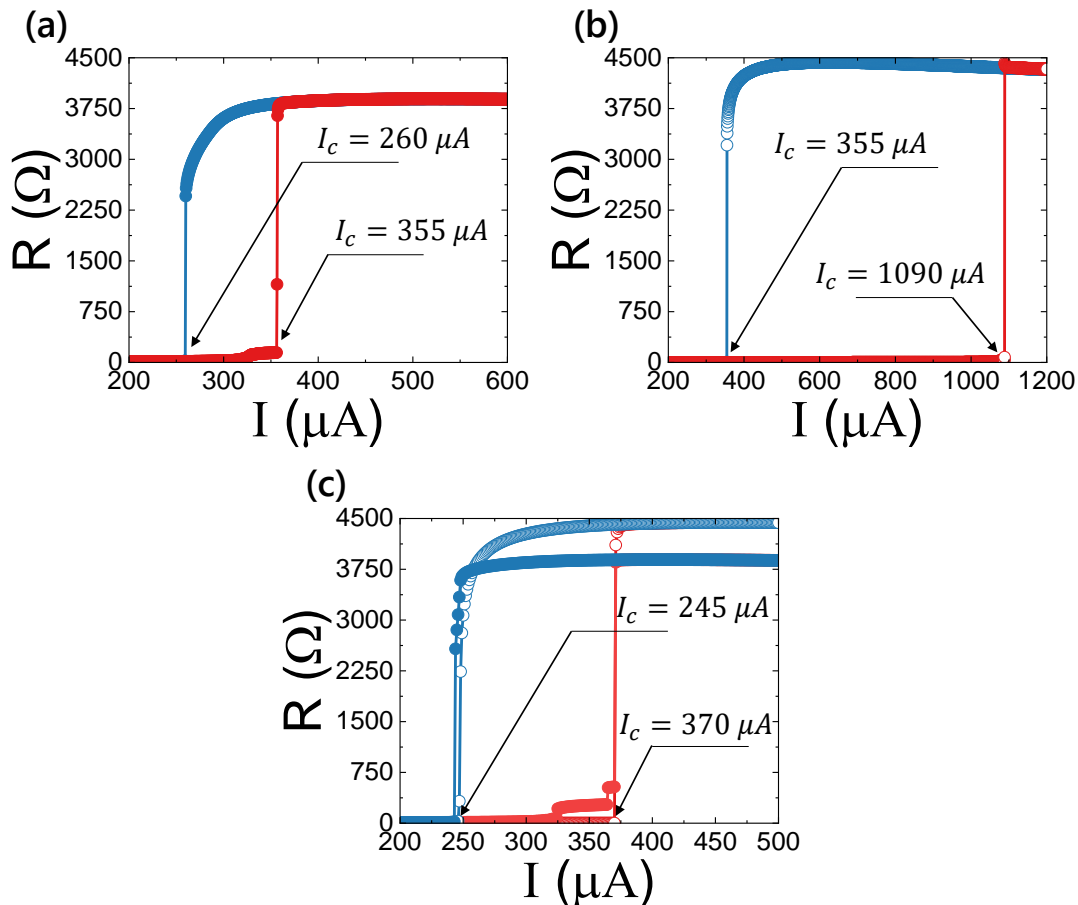


Figure 5.5: Dependency via substrate - Resistance versus current measurements for a network of size $L = 25$ (a) and a network of size $L = 100$ (b) as they are measured *separately*. Blue is for decreasing currents (i.e, N-S PT) and red is for increasing currents (i.e, S-N PT). The critical values of current are clearly different between both networks. (c) Both networks are measured *simultaneously*, causing a mutual PT of both systems, with critical current values that are different from the separate case.

exhibit an abrupt and hysteretic transition at distinct critical current values that differ from each other, as seen in Fig. 5.5a,b. On the contrary, when the networks

are measured *simultaneously*, they experience a *mutual* PT, as seen in Fig 5.5c, at critical current values similar to those in 5.5a, indicating dependency between them, analogous to the case of ISN where the networks are placed one on top of the other and are separated by an insulating medium. In addition to these measurements, we also conducted dynamic measurements on these two networks and discovered that the type of PT they mutually undergo can be tuned and controlled. This is shown and explained in the Appendix.

To further demonstrate the ability of the substrate to induce dependency, we compared two sets of networks (a small network and a large one per each set), fabricated on different substrates, silicon and glass, that have different thermal conductivity values, $\kappa_{\text{silicon}} \approx 500 \frac{W}{m \cdot K}$ [27] and $\kappa_{\text{glass}} \approx 0.01 \frac{W}{m \cdot K}$ [28] at $T = 2$ K, as seen in Fig. 4.3c (S3 configuration). The results for resistance versus temperature measurements are presented in Fig. 5.6.

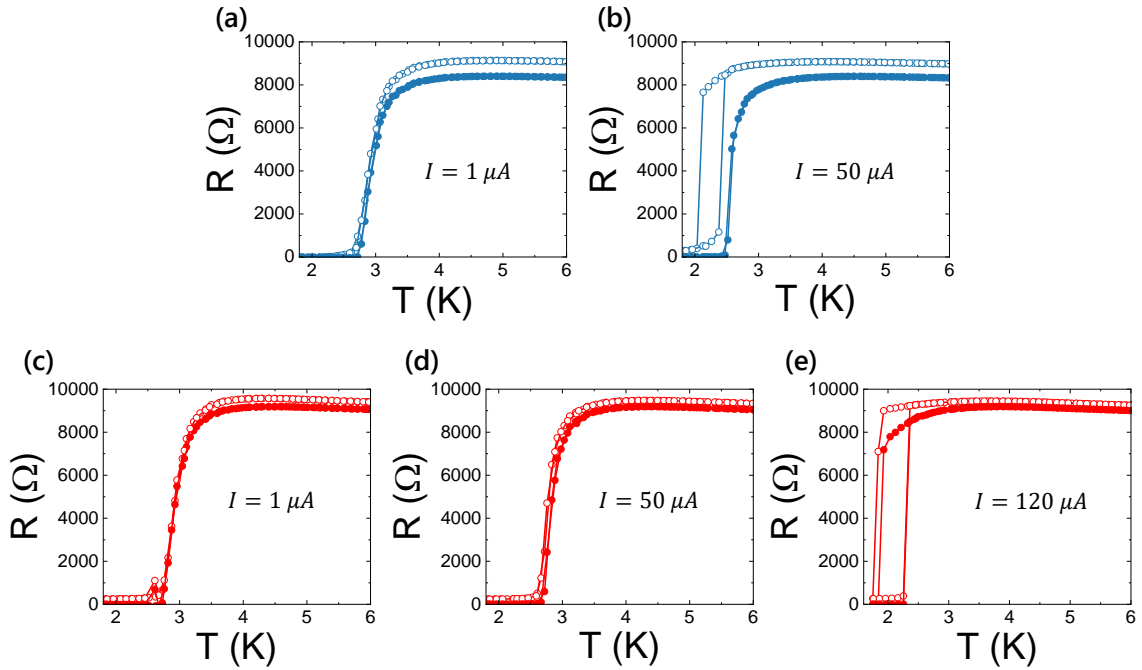


Figure 5.6: Dependency strength - Resistance versus temperature measurements for two networks on glass (blue) and two networks on silicon (red). Full symbols represent a large network ($L = 200$), and empty symbols represent a small network ($L = 25$). At low currents ($I = 1 \mu A$) (a),(c), both pairs of networks behave the same, regardless of the substrate, and continuous PTs are observed. At higher currents ($I = 50 \mu A$), the behavior of the networks depends on the substrate: on glass (b), the small network undergoes an abrupt and hysteretic PT while the large network shows a continuous PT. On silicon (d), both networks exhibit continuous PTs. For higher currents ($I = 120 \mu A$), the silicon networks (e) undergo a mutual abrupt and hysteretic PT, whereas the glass networks do not display a PT within the measured temperature range.

Here, both pairs are measured simultaneously. It is seen that for low currents ($I = 1 \mu\text{A}$), all networks exhibit a continuous PT as seen in Fig. 5.6a,c regardless of the substrate. However, when current values are higher ($I = 50 \mu\text{A}$), the behavior becomes substrate-dependent. On glass (Fig. 5.6b), the smaller network shows an abrupt and hysteretic PT, while the larger network displays a continuous PT. These transitions occur separately from one another. In contrast, on silicon (Fig. 5.6d), both networks exhibit a continuous PT. At higher currents ($I = 120 \mu\text{A}$), the networks on silicon (Fig. 5.6e) undergo a mutual abrupt and hysteretic PT. Under the same conditions, the networks on glass do not show a PT within the measured temperature range.

Next, we aim to show the effect the substrate has on the PT of a single network. To investigate this, we performed transport measurements on two identical networks fabricated on different substrates (S3 configuration). The first on silicon, and the second on glass. The results are shown in Fig. 5.7a.

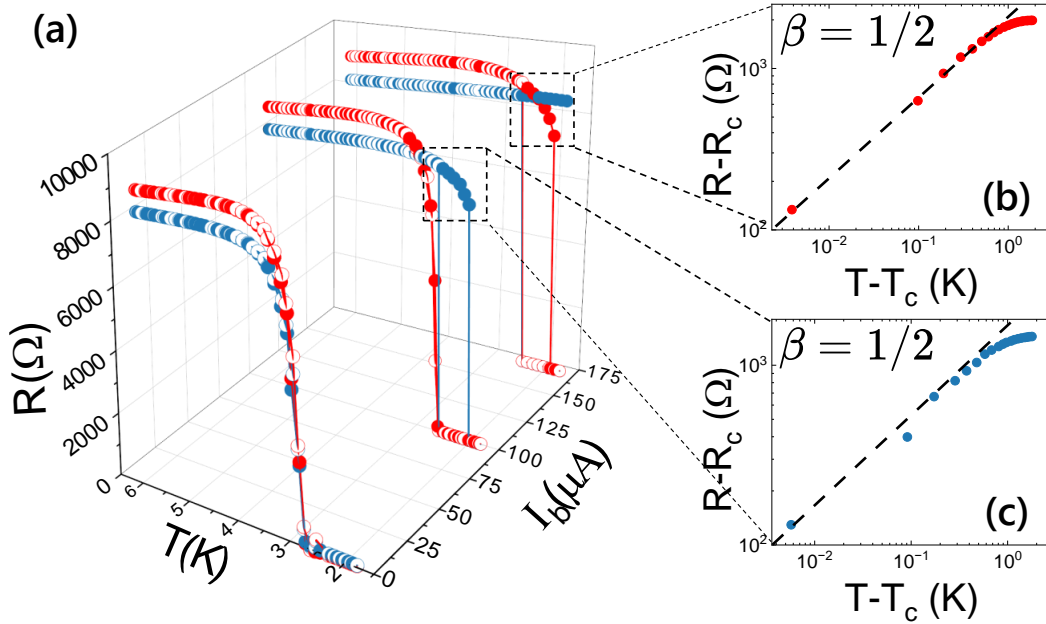


Figure 5.7: Substrate dependence- (a) Experimental resistance versus temperature measurements for a single network, at different bias currents, fabricated on silicon (red symbols) and glass (blue symbols). Full symbols are for cooling cycles and empty symbols are for heating cycles. (b), (c) The extraction of the critical exponent β from the cooling curves of glass and silicon at $I_b = 100 \mu\text{A}$ and $I_b = 170 \mu\text{A}$ respectively.

At low bias currents, where heat generation is insufficient, both networks undergo a continuous, second-order PT from N to S and vice versa. As the bias current is increased, the TISS on glass exhibits an abrupt, hysteretic PT, while the TISS on silicon still undergoes a continuous transition. With further increases of bias cur-

rent, the TISS on silicon also displays an abrupt, hysteretic PT.

We emphasize that for both networks, when the bias current is high enough, an abrupt transition from the N-state to the S-state is observed. This transition is accompanied by the same critical behavior and scaling relation described by Eq. 4, with $\beta = 1/2$, as seen in Fig. 5.7b,c, indicative of a similar mixed-order PT for both TISSs.

The importance of heat transfer can further be appreciated by studying the dependence of the critical temperatures, T_c , for both cooling (N-S transition) and heating (S-N transition) processes, on the bias current. The results for the two substrate samples are shown in Fig. 5.8. It is seen that for the cooling process, the glass

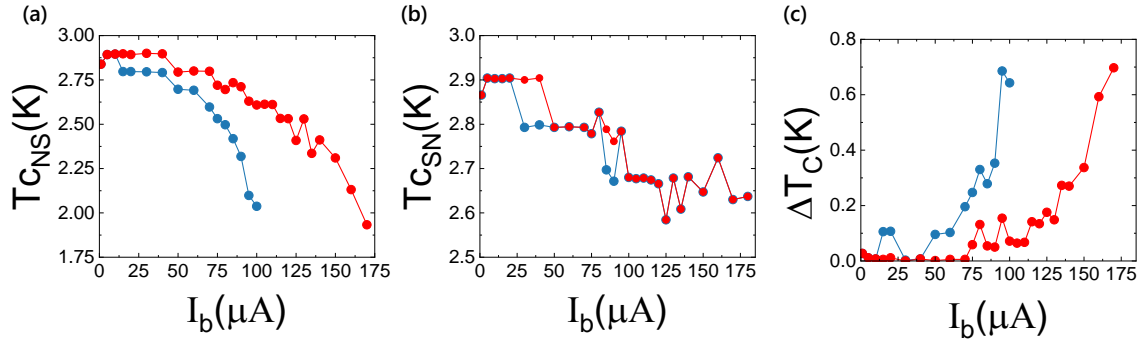


Figure 5.8: Critical temperatures- Critical temperatures of the transitions from N to S (a) (Cooling) and S to N (b) (heating). The hysteresis width is calculated for each bias current measurement (c).

TISS T_c s are consistently smaller than those of the silicone TISS for the same I_b s, demonstrating the larger heat retention of the glass substrate (Fig. 5.8a). On the contrary, during the heating process, for which the S-N PT occurs before heat dissipation diffuses in the system, the T_c s for both networks are not very different (Fig. 5.8b). We note that despite the quantitative difference in heat transfer, the two samples exhibit similar qualitative behavior such as a similar hysteretic nature of critical temperatures with similar temperature differences, $\Delta T = T_c^{SN} - T_c^{NS}$, as seen in Fig. (Fig. 5.8c).

6 Discussion and Conclusions

Our experimental study demonstrates that a TISS can reproduce similar mixed-order PTs previously observed in ISN. This finding represents a conceptual shift in the field of interdependent networks: complex interdependent behavior does not require two structurally distinct networks but can emerge intrinsically within a single homogeneous system, provided it contains two types of interactions.

Comparison of TISS and ISN

In Section 5.1.1, we showed that both ISN and TISS display abrupt, hysteretic PTs at sufficiently high driving currents, accompanied by critical scaling with $\beta = 1/2$ (Eq. 4). At low currents, both systems undergo continuous PTs, while the emergence of heat-induced dependency leads to a mixed-order transition. Notably, TISS required higher driving currents than ISN to generate this dependency, consistent with the fewer amount of heat-emitting segments it contains compared to ISN. These findings support the conclusion that dual interaction mechanisms, connectivity and dependency, are sufficient to generate mixed-order PTs, whether the system consists of two distinct networks or a single network.

Dynamics and Critical Scaling

Resistance versus time measurements (Section 5.1.2) reveal long-lived plateaus as the driving current in the system approaches criticality. The plateau duration, τ , scales with $I - I_c$ (Eq. 6), with the critical exponent $\zeta = 1/2$, and also scales with system size N (Eq. 7) with $\psi = 1/3$. These results are consistent for both ISN and TISS, confirming that both systems share the same critical dynamics. The interpretation of these plateaus as manifestations of microscopic branching cascades aligns with theoretical models of interdependent networks, where local failures trigger long-range cascading events. Our results thus provide experimental evidence that such microscopic dynamics can govern PTs in TISS similar to the results previously observed in ISN.

Different System Sizes

Measurements on networks with sizes ranging from $L = 25$ to $L = 400$ (Section 5.2) show that both small ($L = 25$) and large ($L = 400$) systems exhibit the same critical exponents ($\beta = 1/2$, $\zeta = 1/2$). While the absolute current values required to induce abrupt PTs differ with size, the scaling behavior remains universal. This leads to the conclusion that the mixed-order PT mechanism is insensitive to geometric variations and reflects the intrinsic universality of the dual-interaction framework.

Substrate Dependence and Heat Transfer

We further demonstrated that the substrate thermal conductivity plays a central role in controlling dependency interactions (Section 5.3). We divide the discussion of this section into two parts. The first is the effect the substrate has on dependency *between two distinct* networks. Fig. 5.5 shows that two networks fabricated side by side on a common substrate can undergo a mutual abrupt PT due to substrate-conducted heat flow, while when measured separately, they display distinct transitions. Fig. 5.6 demonstrates that the strength of this coupling depends on the substrate: for a relatively low driving current, when the networks are placed on a glass substrate (low κ), they remain decoupled, while on silicon (high κ) they can couple strongly and undergo a mutual abrupt PT.

The second part of the discussion is the substrate effect on single network systems which exhibit a substrate dependence that might seem the opposite at first glance. Fig. 5.7 shows that on glass, a TISS undergoes abrupt and hysteretic transitions at relatively low bias currents, while on silicon, the same behavior only appears at higher currents. The explanation for this is that a substrate with low thermal conductivity enhances the heat retention of the system, increasing the inter-segment coupling via temperature rise, thus promoting abrupt transitions at lower driven currents. Conversely, a high thermal conductivity substrate allows more efficient heat dissipation (and loss) through the substrate, requiring higher currents to observe similar behavior.

We suggest a basic model to analyze this. Consider a square film of InO at thickness d_f with an area of $A = L^2$ and thermal conductivity k_f placed on a substrate at thickness d_s with thermal conductivity k_s . At this configuration, we can calculate three different heat conductivities, as illustrated in Fig. 6.1:

1. $\sigma_1 = \frac{k_s A}{d_s}$ is the vertical heat conductivity, through the substrate, into the heat bath.
2. $\sigma_2 = \frac{k_s d_s L}{L} = k_s d_s$ is the in-plane heat conductivity through the substrate.
3. $\sigma_3 = \frac{k_f d_f L}{L} = k_f d_f$ is the in-plane heat conductivity through the film.

in our samples,

$$L \approx 10^{-3} \text{ m}, \quad d_s \approx 10^{-4} \text{ m}, \quad d_f \approx 10^{-9} \text{ m}$$

This yields that $\sigma_1 \gg \sigma_2, \sigma_3$, thus indicating that the majority of the heat produced by the film flows to the heat bath, outside of the sample. For a steady electrical power P dissipated in the film, the steady-state temperature rise is

$$\Delta T = \frac{P}{\sigma_{\text{tot}}} \simeq \frac{P}{\sigma_1} = \frac{P d_s}{k_s A} \quad (\text{using } d_s < L \text{ and } \sigma_1 \gg \sigma_2, \sigma_3). \quad (8)$$

Let C_v denote the substrate volumetric heat capacity. The steady energy stored in the substrate is therefore

$$Q_{\text{sub}} = C_v (A d_s) \Delta T \simeq C_v \frac{P d_s^2}{k_s}. \quad (9)$$

Inserting

$$\kappa_{\text{silicon}} \approx 500 \frac{\text{W}}{\text{m K}} \quad C_{\text{silicon}} \approx 4.8 \frac{\text{J}}{\text{m}^3 \text{K}} [29] \quad \kappa_{\text{glass}} \approx 0.01 \frac{\text{W}}{\text{m K}} \quad C_{\text{glass}} \approx 60 \frac{\text{J}}{\text{m}^3 \text{K}} [30]$$

into Eq. 9 yield,

$$\frac{Q_{\text{silicon}}}{Q_{\text{glass}}} = \frac{C_{\text{silicon}} \kappa_{\text{glass}}}{C_{\text{glass}} \kappa_{\text{silicon}}} \rightarrow \boxed{Q_{\text{glass}} = 625000 * Q_{\text{silicon}}}$$

For $d_s < L$, our model is effectively dominated by the vertical heat flow, so the steady-state energy retained in the substrate scales inversely with the substrate thermal conductivity k_s . Consequently, for the same P and d_s , replacing a glass substrate ($\kappa \approx 0.01 \text{ W m}^{-1} \text{ K}^{-1}$) with silicon ($\kappa \approx 500 \text{ W m}^{-1} \text{ K}^{-1}$) reduces the retained energy by roughly 6×10^5 , strongly suppressing heat-mediated coupling and any associated hysteresis.

We note that at sufficiently high currents, both substrates ultimately produce abrupt transitions.

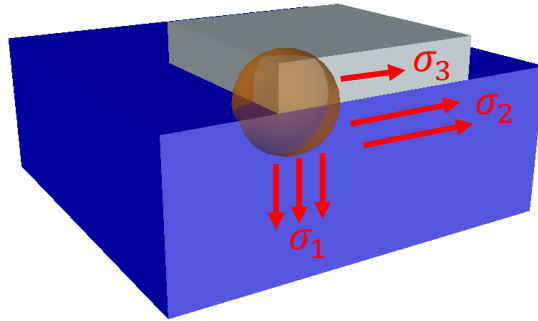


Figure 6.1: Heat flow -A sketch illustrating how heat generated in a segment spreads throughout the sample. σ_1 is the heat conductivity flowing to the heat bath, perpendicular to the substrate. σ_2, σ_3 are the heat conductivity flowing in-plane, through the substrate and the sample, respectively.

Finally, Fig. 5.8 provides further evidence for this mechanism: the critical temperature during cooling (T_c^{NS}) is consistently lower for TISS on glass than on silicon, reflecting greater in-plane heat retention, which in turn enhances dependency. In contrast, during heating (T_c^{SN}), where prior to the PT essentially no heat is produced and thus dependency is scarce, the networks on different substrates show similar results. Both networks, however, exhibit similar hysteresis widths $\Delta T = T_c^{SN} - T_c^{NS}$, confirming that while the substrate affects the heat needed to generate dependency, the overall mixed-order nature of the PT remains unchanged.

Together, these results confirm the thermal origin of the dependency interaction, in superconducting networks, and identify substrate conductivity as a practical tuning parameter. By modulating heat retention and dissipation, the substrate dictates the current threshold at which continuous PTs transit to mixed-order PTs. In addition, in systems with several networks, it governs the coupling strength between them.

Universality and Broader Implications

Throughout all of our experimental configurations, ISN and TISS exhibited identical critical exponents ($\beta = 1/2$, $\zeta = 1/2$, $\psi = 1/3$). These universal scaling behaviors suggest that the microscopic mechanism is independent of system geometry or implementation. Our work therefore supports the broader idea that mixed-order PTs arise whenever short-range connectivity is coupled to long-range dependency, regardless of physical realization. While our focus was on superconducting networks, we propose that the principle may extend to other physical systems, whenever the dual-interaction mechanism naturally emerges. For example: traffic systems (roads vs. congestion), neural networks (synaptic vs. modulatory signals), and materials (bonding vs. phonons). Clearly, work on other types of TISS is required to test this hypothesis.

This study demonstrates that abrupt PTs and cascading dynamics, previously attributed to the interdependency between distinct networks, can also occur in a single network system, through interdependency between its elements. This reduces the fabrication complexity of experimental realizations while broadening the applicability of interdependent network theory. Moreover, dependency interactions can be continuously tuned, by current (see Appendix) or substrate choice, offering a practical route to engineer PT characteristics. This tunability could enable the design of devices such as sensors that exploit the sharpness and criticality of mixed-order transitions.

In summary, our experiments establish TISS as a physical platform for studying interdependent-like behavior, validate the universality of mixed-order PT scaling across geometries and substrates, and point toward new opportunities for engineered phase-switching systems.

7 Future Research

While this work establishes single superconducting networks (TISS) as a platform for mixed-order phase transitions, several open questions remain and motivate future investigations.

First, the role of substrate-induced coupling deserves deeper exploration. We demonstrated that thermal conductivity controls the onset of abrupt transitions (Fig. 5.5 and Fig. 5.8), but additional study across substrates with tunable thermal properties could assess this dependency more precisely. For example, graphene, encapsulated by an electrically insulating material, could be a suitable candidate. By gating the graphene, one can control its charge carrier density, which at cryogenic temperatures, can have an impact on its thermal conductivity [31–33]. Measuring a superconducting system’s behavior on such a substrate, during a continuous alternation of its thermal conductivity, could offer new insights on these substrate dependencies.

Second, the dynamics of the resistance plateaus raise important open questions: What is the physical mechanism that causes the resistance to fluctuate during the long-lived plateau?; Are the cascading avalanches of phase changes restricted to only certain areas in the system?; Can different forms of collapse be found during the transition? While our data support a branching-cascade origin, direct microscopic probes (e.g., spatially resolved thermal imaging, local resistance mapping, and scanning SQUID microscopy) could test this mechanism more explicitly. Linking microscopic changes to the macroscopic scaling laws would further bridge the gap between experiment and interdependent network theory.

Third, the exploration of material platforms beyond superconductors is a promising avenue. Extending to other materials could test the generality of the dual-interaction mechanism beyond superconductivity and heat dissipation. For example, we suggest a system that includes a granular ferromagnetic film where electric conductivity may serve as connectivity links and magnetic interactions could act as dependency links. This system, which is physically different from superconducting networks, may exhibit different thresholds or scaling behaviors.

Finally, our findings motivate the development of device-oriented studies. The ability to tune critical temperatures and hysteresis widths by substrate engineering (Fig. 5.8) suggests applications in sensors, detectors, or adaptive circuits. Future research could focus on quantifying switching speed, noise sensitivity, and stability under repeated cycling to evaluate technological feasibility.

In summary, future research should expand the substrate effect, deepen microscopic understanding of dynamics, explore alternative material platforms, and investigate device-oriented implementations. Together, these directions can both refine our understanding of mixed-order transitions and move toward practical exploitation of their unique properties.

8 Appendix

Here, we show dynamic measurements that were conducted on the networks in Section 5.3. We discovered that the dependency interaction strength can be controlled as a tuning parameter that governs the coupling between the two networks and affects the PT they undergo. This is demonstrated in Fig. 8.1, which shows resistance versus time measurements for the two networks as they are measured simultaneously. When the current through the large network is low (Fig. 8.1a), the two networks

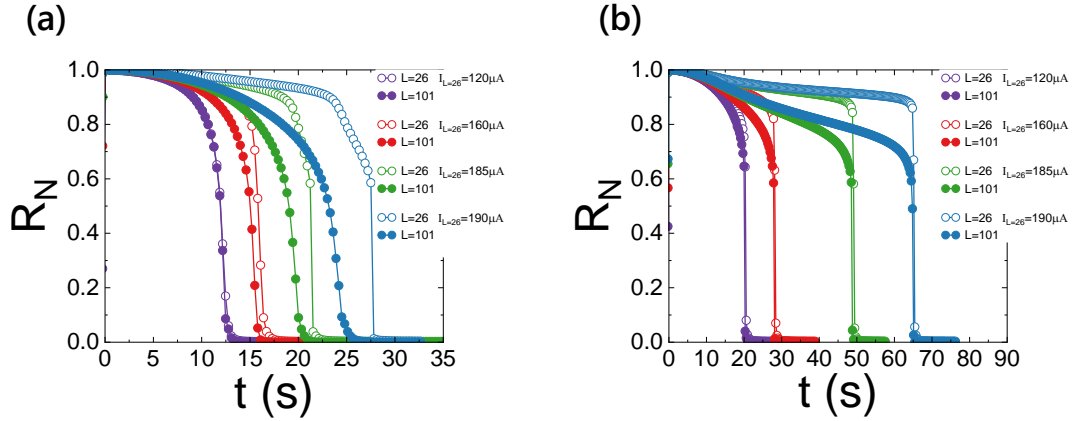


Figure 8.1: Tuning the PT - Resistance versus time measurements for two networks on the same substrates. Full symbols are for the large network ($L = 100$) and empty symbols are for the small network ($L = 25$). Both networks are measured simultaneously during the procedure described in section 4.2.2. **(a)** Low driven current of the large network. As the driven current in the small network raises, it develops an abrupt transition while the large network transition remains continuous, as both networks transitions gets separated from each other. **(b)** High driven current of the large network. Here, both networks undergo a mutual, abrupt transition, regardless of the current of the small network.

behave differently as the current of the small network raises. It is seen that while the transition of the small network becomes abrupt, as the current of it raises, the transition of the large network remains continuous. In this regime, the transitions of the two networks are separated in time, which indicates a weak coupling between them. In contrast, when the current through the large network is high (Fig. 8.1b), both the large and small networks exhibit simultaneous abrupt transitions regardless of the current of the small network. This indicates a strong coupling regime between the networks. These findings, which were first discovered in the frame of this work, became the foundation for additional research that focused on the *range of the dependency* between ISN, which was the main subject of other lab members' research. They demonstrate that the inter-network interactions, controlled here by the drive current through the large network, can tune the nature of the PT from decoupled continuous and abrupt transitions to a mutually abrupt transition.

Reference

- [1] James P. Sethna. *Entropy, order parameters, and complexity*. Oxford University Press, 2006.
- [2] Mark W. Zemansky and Richard H. Dittman. *Heat and thermodynamics*. McGraw-Hill book company, 1981.
- [3] Stanley H. Eugene. *Introduction to phase transitions and critical phenomena*. Clarendon Press, 1971.
- [4] C. Domb. *Phase transitions and critical phenomena*. Elsevier, 2000.
- [5] J. Gao, S. V. Buldyrev, Havlin Shlomo, and H. E. Stanley. “Robustness of a Network of Networks”. In: *Phys. Rev. Lett.* 107 (2011), p. 195701.
- [6] Sergey V. Buldyrev, Roni Parshani, Gerald Paul, H. Eugene Stanley, and Shlomo Havlin. “Catastrophic cascade of failures in interdependent networks”. In: *Nature* 464 (2010), pp. 1025–1028.
- [7] M. M. Danziger, L. M. Shekhtman, A. Bashan, Y. Berezin, and S. Havlin. “Vulnerability of Interdependent Networks and Networks of Networks”. In: *Interconnected Networks* (2016), p. 79.
- [8] J. Gao, S. V. Buldyrev, H. E. Stanley, and Havlin Shlomo. “Networks formed from interdependent networks”. In: *Nature Physics* 8.1 (2012), pp. 40–48.
- [9] Jianxi Gao, Amir Bashan, Louis Shekhtman, and Shlomo Havlin. *Introduction to Networks of Networks*. 2053-2563. IOP Publishing, 2022. ISBN: 978-0-7503-1046-8. DOI: 10.1088/978-0-7503-1046-8. URL: <https://dx.doi.org/10.1088/978-0-7503-1046-8>.
- [10] Michael M Danziger, Amir Bashan, Yehiel Berezin, and Shlomo Havlin. “Percolation and cascade dynamics of spatial networks with partial dependency”. In: *Journal of Complex Networks* 2.4 (2014), pp. 460–474.
- [11] Michael M Danziger, Ivan Bonamassa, Stefano Boccaletti, and Shlomo Havlin. “Dynamic interdependence and competition in multilayer networks”. In: *Nature Physics* 15.2 (2019), pp. 178–185.
- [12] Davide Cellai, Eduardo López, Jie Zhou, James P. Gleeson, and Ginestra Bianconi. “Percolation in multiplex networks with overlap”. In: *Phys. Rev. E* 88 (5 Nov. 2013), p. 052811. DOI: 10.1103/PhysRevE.88.052811. URL: <https://link.aps.org/doi/10.1103/PhysRevE.88.052811>.

- [13] Davide Cellai, Sergey N. Dorogovtsev, and Ginestra Bianconi. “Message passing theory for percolation models on multiplex networks with link overlap”. In: *Phys. Rev. E* 94 (3 Sept. 2016), p. 032301. DOI: 10.1103/PhysRevE.94.032301. URL: <https://link.aps.org/doi/10.1103/PhysRevE.94.032301>.
- [14] Ivan Bonamassa, Bnaya Gross, and Shlomo Havlin. “Interdependent couplings map to thermal, higher-order interactions”. In: *arXiv preprint arXiv:2110.08907* (2021).
- [15] Deokjae Lee, S. Choi, M. Stippinger, J. Kertész, and B. Kahng. “Hybrid phase transition into an absorbing state: Percolation and avalanches”. In: *Phys. Rev. E* 93 (4 Apr. 2016), p. 042109. DOI: 10.1103/PhysRevE.93.042109. URL: <https://link.aps.org/doi/10.1103/PhysRevE.93.042109>.
- [16] Tanja Holstein, Marc Wiedermann, and Jürgen Kurths. “Optimization of coupling and global collapse in diffusively coupled socio-ecological resource exploitation networks”. In: *New Journal of Physics* 23.3 (Mar. 2021), p. 033027. DOI: 10.1088/1367-2630/abe0db. URL: <https://dx.doi.org/10.1088/1367-2630/abe0db>.
- [17] S. Boccaletti, G. Bianconi, R. Criado, C.I. del Genio, J. Gómez-Gardeñes, M. Romance, I. Sendiña-Nadal, Z. Wang, and M. Zanin. “The structure and dynamics of multilayer networks”. In: *Physics Reports* 544.1 (2014). The structure and dynamics of multilayer networks, pp. 1–122. ISSN: 0370-1573. DOI: <https://doi.org/10.1016/j.physrep.2014.07.001>. URL: <https://www.sciencedirect.com/science/article/pii/S0370157314002105>.
- [18] Antonios Garas. *Interconnected Networks*. Springer, 2016.
- [19] Ginestra Bianconi. *Multilayer Networks: Structure and Function*. Oxford University Press, 2018.
- [20] Mikko Kivelä, Alex Arenas, Marc Barthelemy, James P. Gleeson, Yamir Moreno, and Mason A. Porter. “Multilayer networks”. In: *Journal of Complex Networks* 2.3 (July 2014), pp. 203–271.
- [21] Juan C. Rocha, Garry Peterson, Örjan Bodin, and Simon Levin. “Cascading regime shifts within and across scales”. In: *Science* 362.6421 (2018), pp. 1379–1383. DOI: 10.1126/science.aat7850. eprint: <https://www.science.org/doi/pdf/10.1126/science.aat7850>. URL: <https://www.science.org/doi/abs/10.1126/science.aat7850>.

- [22] I. Bonamassa, B. Gross, M. Laav, I. Volotsenko, A. Frydman, and S. Havlin. “Interdependent superconducting networks”. In: *Nature Physics* 19 (2023), pp. 1163–1170.
- [23] Bnaya Gross, Irina Volotsenko, Yuval Sallem, Nahala Yadid, Ivan Bonamassa, Shlomo Havlin, and Aviad Frydman. “The random cascading origin of abrupt transitions in interdependent systems”. In: *Nature Communications* 16 (2025), p. 5869. DOI: 10.1038/s41467-025-61127-z. URL: <https://doi.org/10.1038/s41467-025-61127-z>.
- [24] Bnaya Gross, Hillel Sanhedrai, Louis Shekhtman, and Shlomo Havlin. “Interconnections between networks acting like an external field in a first-order percolation transition”. In: *Phys. Rev. E* 101 (2 Feb. 2020), p. 022316. DOI: 10.1103/PhysRevE.101.022316. URL: <https://link.aps.org/doi/10.1103/PhysRevE.101.022316>.
- [25] Bnaya Gross, Ivan Bonamassa, and Shlomo Havlin. “Microscopic Intervention Yields Abrupt Transition in Interdependent Ferromagnetic Networks”. In: *Phys. Rev. Lett.* 132 (22 May 2024), p. 227401. DOI: 10.1103/PhysRevLett.132.227401. URL: <https://link.aps.org/doi/10.1103/PhysRevLett.132.227401>.
- [26] Dong Zhou, Amir Bashan, Reuven Cohen, Yehiel Berezin, Nadav Shnerb, and Shlomo Havlin. “Simultaneous first- and second-order percolation transitions in interdependent networks”. In: *Phys. Rev. E* 90 (1 July 2014), p. 012803. DOI: 10.1103/PhysRevE.90.012803. URL: <https://link.aps.org/doi/10.1103/PhysRevE.90.012803>.
- [27] J.C. Thompson and B.A. Younglove. “Thermal conductivity of silicon at low temperatures”. In: *Journal of Physics and Chemistry of Solids* 20.1 (1961), pp. 146–149. ISSN: 0022-3697. DOI: [https://doi.org/10.1016/0022-3697\(61\)90146-9](https://doi.org/10.1016/0022-3697(61)90146-9). URL: <https://www.sciencedirect.com/science/article/pii/0022369761901469>.
- [28] M. P. Zaitlin and A. C. Anderson. “Thermal Conductivity of Borosilicate Glass”. In: *Phys. Rev. Lett.* 33 (19 Nov. 1974), pp. 1158–1161. DOI: 10.1103/PhysRevLett.33.1158. URL: <https://link.aps.org/doi/10.1103/PhysRevLett.33.1158>.
- [29] P. D. Desai. “Thermodynamic Properties of Iron and Silicon”. In: *Journal of Physical and Chemical Reference Data* 15.3 (July 1986), pp. 967–983. ISSN: 0047-2689. DOI: 10.1063/1.555761. eprint: <https://pubs.aip.org/aip/>

jpr/article-pdf/15/3/967/11572421/967_1_online.pdf. URL: <https://doi.org/10.1063/1.555761>.

- [30] R. C. Zeller and R. O. Pohl. “Thermal Conductivity and Specific Heat of Noncrystalline Solids”. In: *Phys. Rev. B* 4 (6 Sept. 1971), pp. 2029–2041. DOI: 10.1103/PhysRevB.4.2029. URL: <https://link.aps.org/doi/10.1103/PhysRevB.4.2029>.
- [31] S. Yiğen and A. R. Champagne. “Wiedemann–Franz Relation and Thermal-Transistor Effect in Suspended Graphene”. In: *Nano Letters* 14.1 (Dec. 2013), pp. 289–293. ISSN: 1530-6992. DOI: 10.1021/nl403967z. URL: <http://dx.doi.org/10.1021/nl403967z>.
- [32] Kin Chung Fong and K. C. Schwab. “Ultrasensitive and Wide-Bandwidth Thermal Measurements of Graphene at Low Temperatures”. In: *Phys. Rev. X* 2 (3 July 2012), p. 031006. DOI: 10.1103/PhysRevX.2.031006. URL: <https://link.aps.org/doi/10.1103/PhysRevX.2.031006>.
- [33] L. Palma-Chilla and J.C. Flores. “Direct/Dual electronic thermal conductivity on graphene: Gate-potential and ripples”. In: *Physica B: Condensed Matter* 577 (2020), p. 411828. ISSN: 0921-4526. DOI: <https://doi.org/10.1016/j.physb.2019.411828>. URL: <https://www.sciencedirect.com/science/article/pii/S0921452619307197>.